ACS APPLIED MATERIALS & INTERFACES

Forum Article

www.acsami.org

Phoxonic Hybrid Superlattice

Elena Alonso-Redondo,[†,‡] Hannah Huesmann,[†,§] El-Houssaine El Boudouti,[⊥,#] Wolfgang Tremel,[§] Bahram Djafari-Rouhani,[#] Hans-Juergen Butt,[‡] and George Fytas*[,‡,∥]

[‡]Max Planck Institute for Polymer Research, Ackermannweg 10, 55128 Mainz, Germany

[§]Department of Inorganic Chemistry, Johannes Gutenberg University, Duesbergweg 10-14, 55128 Mainz, Germany

[⊥]LDOM, Département de Physique, Faculté des Sciences, Université Mohamed I, 60000 Oujda, Morocco

[#]Institut d'Électronique, de Microélectronique et de Nanotechnologie (IEMN), UMR-CNRS 8520, UFR de Physique, Université de Lille 1, 59655 Villeneuve d'Ascq, France

[∥]Department of Materials Science, University of Crete and IESL/FORTH, 71110 Heraklion, Greece

ABSTRACT: We studied experimentally and theoretically the direction-dependent elastic and electromagnetic wave propagation in a supported film of hybrid PMMA (poly[methyl-methacrylate])-TiO_2 superlattice (SL). In the direction normal to the layers, this one-dimensional periodic structure opens propagation band gaps for both hypersonic (GHz) phonons and near-UV photons. The high mismatch of elastic and optical impedance results in a large dual phoxonic band gap. The presence of defects inherent to the spin-coating fabrication technique is sensitively manifested in the band gap region. Utilizing Brillouin light scattering, phonon propagation along the layers was observed to be distinctly different from propagation normal to them and can, under certain conditions (SL thickness and substrate elasticity), reveal the nanomechanical properties of the constituent layers. Besides the first realization of unidirectional phoxonic behavior, hybrid (soft−hard) periodic materials are a promising simple platform for opto-acoustic interactions and applications such as filters and Bragg mirrors.

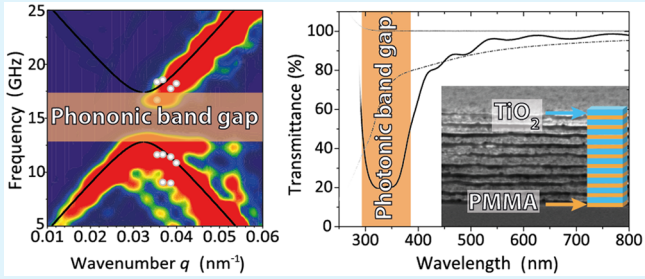

KEYWORDS: *hybrid superlattices, band gap, phononics, photonics, Brillouin spectroscopy*

INTRODUCTION

Properties of periodic nanocomposites differ from those of their bulk constituents. The flow of elastic and electromagnetic waves is drastically altered by the presence of alternating dissimilar impedances in composite structures. The destructive interference along the periodicity direction opens frequency band gaps that prohibit wave propagation. This property can be exploited to develop and customize materials with designed mechanical and optical characteristics. Potential applications of periodic structures include their use as Bragg reflectors for nonabsorbing laser cavity mirrors[1] as humidity and liquid sensors[2,3] or for thermal management.[4−6] In particular, polymer composites are attractive because of their elasticity, transparency and easy fabrication. Despite the closeness of the refractive indices, photonic applications incorporating polymers are well-established. For example, this is the case of the microsegregated block copolymers.[2,7,8] Yet, to function as phononic materials, a sufficiently large elastic impedance $Z = \rho c$ mismatch (involving two physical quantities, density ρ and sound velocity c) is required for a sizable band gap.[9−12] Inorganic materials are frequently used to boost the impedance mismatch for a designed phononic and photonic crystal.[13,14] One-dimensional (1D) crystals facilitate the study of elastic wave propagation because of the vector character of the latter.

The majority of experimental investigations deal with inorganic materials such as Si, GaAs, AlAs or Au because molecular beam epitaxy, sputtering or lithography allow for good control over sample thickness and defects.[15−20] In particular, 1D crystals with periodicity normal to the substrate, termed superlattices (SLs), promote both phononic and photonic band gaps. Expansion to hybrid SLs with one soft polymeric phase enlarges the range of elastic impedance. For example, SLs consisting of alternating poly(methyl-methacrylate) (PMMA) and porous silica (SiO_2) nanoparticle layers fabricated by spin coating have advanced our fundamental knowledge in small scale phononics.[10,14,21] The cavity and surface modes as well as their interaction when varying the thickness and the position of the cavity layer were identified by the full theoretical description of the phononic density of states (DOS) recorded by Brillouin light scattering (BLS). In general for SLs, the band gap at normal incidence depends on the c and ρ contrast between the layers. Replacement of the SiO_2 (c_{SiO_2} =

Special Issue: Forum on Polymeric Nanostructures: Recent Advances toward Applications

Received: November 9, 2014
Accepted: April 2, 2015
Published: April 9, 2015

DOI: 10.1021/acsami.5b01247
ACS Appl. Mater. Interfaces 2015, 7, 12488−12495

5660 m/s, ρ_{SiO_2} = 2400 kg/m^3) layer by TiO_2 ($c_{TiO_2,bulk}$ = 8440 m/s, $\rho_{TiO_2,bulk}$ = 3900 kg/m^3) should boost the elastic impedance. The phonon propagation in an almost symmetric TiO_2–PMMA SL with a lattice constant of 0.22 μm was earlier investigated with a photoacoustic technique.[22] In that study, the probed phonon wavelengths ($6 < \Lambda < 30$ μm) are much longer than the lattice constant, and fall within the long wavelength regime far from the band gap region. Hence, this earlier study of phonon propagation along the periodicity direction could not reveal phononic behavior. Instead, the propagation normal to the layers yielded the effective medium elastic properties that unexpectedly resemble those of the PMMA layer.

To achieve large phononic and photonic band gaps, we fabricated a PMMA-TiO_2 SL by spin-coating subsequent layers on a glass substrate. We have chosen a spatial periodicity of $d \approx$ 100 nm and probing phonon wave vector q, with $qd \approx 1$. The periodicity was selected to achieve dual band gap, a near-UV photonic and a hypersonic (GHz) phononic. Also, we probed phonon propagation normal to the periodicity direction using BLS, where no phononic gap but different effective medium behavior is expected. At the nanoscale, confinement and interface effects can render different effective material elastic properties than in the bulk. Experimental results along with theoretical band structure analysis allow a complete optical and nanomechanical characterization of the multilayer structure, thereby settling the necessary fundamental knowledge for applications.

The paper is organized as follows: in Section A, we present the structural characterization of the PMMA-TiO_2 SL. In Section B, we describe how the sound velocity of the constituent layers, measured by BLS, is estimated. In addition, we discuss the conditions under which the effective medium sound velocity of the SL can be obtained from the in-plane BLS spectra. In Section C, we provide the phononic band structure along the periodicity direction and demonstrate the phononic behavior both experimentally and theoretically. In Section D, we characterize the optical transmittance and photonic band structure of the SL, which confirms the dual gap for elastic and electromagnetic waves.

RESULTS AND DISCUSSION

A. Design of Transparent SL. To fabricate our one-dimensional SL, we spin-coated 1D alternating bilayers of PMMA and TiO_2 nanoparticles, in total 20 layers on transparent SiO_2 glass substrate. The polymer used was PMMA (poly [methyl-methacrylate]) with a molecular weight M_w = 35 kg/mol, transparent for the wavelengths of our study and thermally stable. TiO_2 (titania) nanoparticles were chosen because of the large impedance contrast with the PMMA; additionally, the transparency of the TiO_2 in the visible spectrum and strong absorption for the UV light represent advantageous attributes in order to create transparent films and protect the polymer from UV degradation. The diameter of the spherical TiO_2 nanoparticles is ~7 nm, which allows (a) a good dispersion in the solvent for subsequent spin-coating and wettability and (b) several strata of particles, for a homogeneous inorganic layer. PMMA shows a good adhesion to the TiO_2 particles, essential for a stable multilayer composite without voids. The mismatch of elastic and optical properties is large for these compatible components, in comparison with other combinations of polymer and inorganic particles. For example, $LiNbO_3$ (refractive index n = 2.32) has no good performance when spin-coated. Other metals such as gold or lead, despite their high density contrast, have a strong absorption in the visible range, with undesirable effects on the transparency of the superlattice.[13,23] The lattice constant of the SL is $\pi/q \approx$ 100 nm, with q being the wavenumber of the first Brillouin zone (BZ).

The spacing of the layers was determined from cross sectional scanning electron microscopy (SEM) images (Figure 1). The estimated thickness of the PMMA and TiO_2 amounts

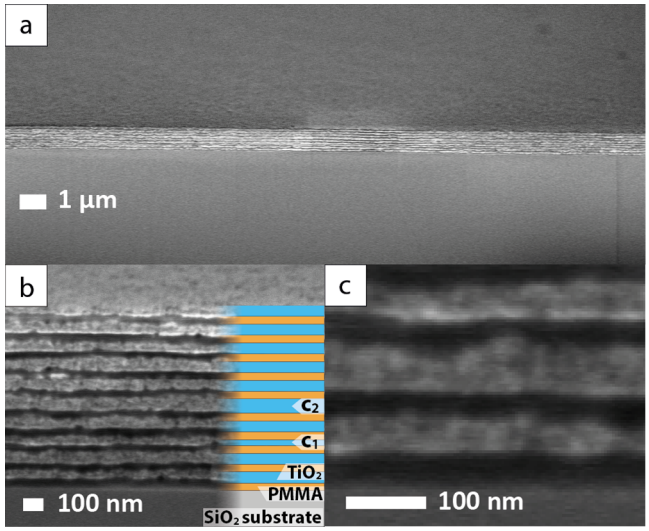

Figure 1. (a) Cross-sectional SEM micrograph of the 10-bilayer PMMA-TiO_2 superlattice. (b) Schematic of the SL. The two cavity defects are noted as c_1 and c_2. (c) High-magnification image showing the substrate (bottom) and subsequent alternating bilayers.

to 40 ± 5 nm and 57 ± 7 nm, respectively, and hence the periodicity is d = 97 ± 6 nm. The shape and ordering of the layers is extended over large areas (Figure 1a). Because of the fabrication technique, there is a nonperfect alternation of the layer spacing in the SL (Figure 1b and 1c), however the bandgap was found to be robust to structural incoherence of few nanometers.[14] We have labeled in Figure 1b the two layers with marked differences, named cavities c_1 and c_2 with thicknesses 30 and 75 nm, respectively. The identification of these cavities is crucial in the theoretical representation of the phononic band structure (next Section C). The small roughness observed in Figure 1c are less than 10% and does not represent an obstacle to achieve large bandgaps, as reported previously.[14] Moreover, the probing spot size (50 μm) is much larger than the length scale of the roughness, affecting mainly the width of the experimental BLS spectra.

B. Constituent Layers and SL in-Plane Propagation. To characterize separately the elastic properties of the constituents, we fabricated additional films of PMMA and TiO_2 alone. The estimation of the sound velocities in the two constituent layers is necessary to reduce the number of adjustable parameters in the theoretical modeling of the phononic dispersion of the SL. We prepared PMMA and TiO_2 nanoparticle films dropcasted from solution. The thickness of the films was in the micrometer range to measure bulk properties and avoid surface modes.[24−26] The dispersion relation in Figure 2b, measured by BLS, is linear (i.e., purely acoustic) as expected for homogeneous films. The longitudinal sound velocity, obtained from the linear slope, amounts to c_{drop}

DOI: 10.1021/acsami.5b01247
ACS Appl. Mater. Interfaces 2015, 7, 12488−12495

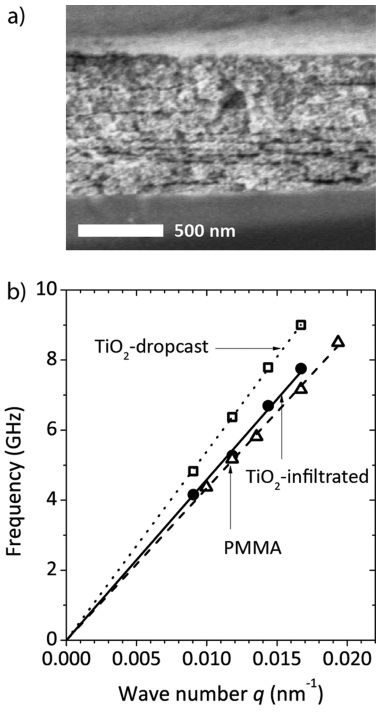

Figure 2. (a) Cross-sectional SEM micrograph of the TiO_2-infiltrated film. (b) Linear (acoustic) dispersion, frequency vs wave vector, for the longitudinal phonon in the TiO_2-infiltrated film (solid circles), TiO_2-dropcasted (open squares) and PMMA (open triangles). The wave vector q is parallel to the film surface. The experimental error for the phonon frequencies amounts 1%.

= 3390 ± 40 m/s in the TiO_2-dropcasted and $c_{L,PMMA}$ = 2730 ± 20 m/s in the PMMA. The low c_{drop} relative to $c_{TiO_2,bulk}$ is due to the porosity of the TiO_2-dropcasted film. In the fabrication of the SL by spin-coating, infiltration of PMMA is unavoidable and hence the c_{drop} value might not be the appropriate estimate of the sound velocity in TiO_2 sublayer of the SL.

To find a better representation of the TiO_2 layer in the SL, we prepared a third film by spin-coating subsequent layers of TiO_2 and a thin layer (1 wt %) of PMMA, up to a total thickness of about 1 μm. PMMA is completely infiltrated in the TiO_2 layer, as confirmed by the SEM image (Figure 2a). In spite of the layering observed in the direction perpendicular to the substrate, this film appears homogeneous, because these local heterogeneities are much smaller than the phonon wavelengths (Λ > 300 nm). Hence a single purely acoustic phonon is observed (Figure 2b) yielding an effective medium sound velocity $c^*_{TiO_2}$ = 2900 ± 50 m/s. The infiltration of PMMA in the porous TiO_2 layer seriously impacts its sound velocity as compared to the $c_{TiO_2,bulk}$ of anatase crystal and even c_{drop} in the TiO_2-dropcasted. Therefore, the access to the experimental $c^*_{TiO_2}$ is crucial.

A similar drop is anticipated for the density $\rho^*_{TiO_2}$ of this layer that affects the elastic impedance. However, since this value can be hardly estimated without serious assumptions on the porosity and composition dependence of the mean density, we deliberately used $\rho^*_{TiO_2}$ as an adjustable parameter that sensitively enters the theoretical description of the SL band structure. From the representation of the experimental dispersion relation (Figure 5 below), we estimated $\rho^*_{TiO_2}$ = 1900 kg/m^3. The values $c^*_{TiO_2}$ and $\rho^*_{TiO_2}$ of the TiO_2-infiltrated film are internally consistent as they can be rationalized by the Wood's effective medium law.[27,28] Using the density and sound velocity of the bulk TiO_2 and PMMA, $c^*_{TiO_2}$ in the TiO_2 infiltrated film can be captured with $\rho^*_{TiO_2}$ assuming 50% of TiO_2 volume fraction. Thus, the TiO_2 infiltrated layer with more than 50% of TiO_2 volume fraction can possess a value of $c^*_{TiO_2}$ only 5% higher than $c_{L,PMMA}$.

The longitudinal sound velocities of the two constituent layers should rationalize the experimental effective $c_{L,eff}$ for in-plane propagation in the SL. Along this direction, normal to the periodicity, there are several possible elastic excitations depending on the film thickness[24,26,29,30] rendering Wood's effective medium law inappropriate. On the experimental side, the BLS spectra (~12 h acquisition) display a single phonon structure as shown in Figure 3a (for the anti-Stokes side). The

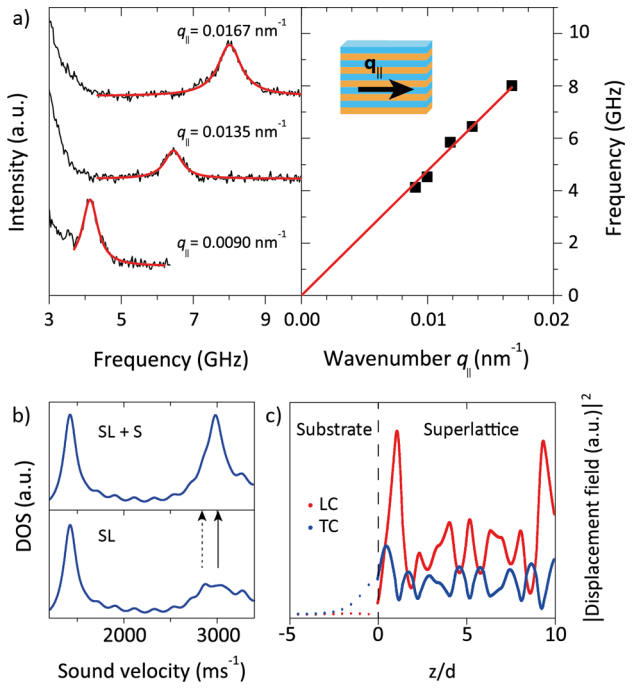

Figure 3. (a) BLS spectra recorded parallel to the substrate (normal to the periodicity) at three wave vectors $q_\parallel$ as indicated in the plot. The spectra are well-represented by a single Lorentzian shape (red line) and the peak frequency is plotted against $q_\parallel$ in the right panel. The pure acoustic nature of the phonon is indicated by the solid red line. (b) Computed total density of states (DOS) integrated over the thickness of SL and substrate (top) and only in the SL (bottom). The two arrows indicate the frequencies of the experimental longitudinal sound velocity c_L = 3010 m/s phonon (solid) and the computed effective medium sound velocity $c_{L,eff}$ = 2840 m/s (dashed) at $q_\parallel$ = 0.0167 nm^{-1}. (c) Square modulus of the displacement fields of the acoustic modes around 3000 m/s in the supported SL with longitudinal (LC, red line) and transverse (TC, blue line) components of the polarization against the dimensionless z/d position.

frequency f at the peak position increases linearly with $q_\parallel$ (right panel of Figure 3a) yielding the longitudinal sound velocity c_L = $2\pi f/q_\parallel$ = 3010 ± 40 m/s. Unexpectedly, this value exceeds both $c^*_{TiO_2}$ and $c_{L,PMMA}$ of the infiltrated TiO_2 and PMMA layers and cannot represent the effective medium longitudinal velocity $c_{L,eff}$ of the SL. We note that for a similar SL (infiltrated SiO_2/PMMA),[14] c_L falls between the sound velocities of the two

DOI: 10.1021/acsami.5b01247
ACS Appl. Mater. Interfaces 2015, 7, 12488−12495

sublayers and a good agreement with $c_{L,eff}$ was reported. The latter can be theoretically estimated for an infinite PMMA-TiO_2 SL using essentially c^*_{TiO2} and $c_{L,PMMA}$ with minor effect of the corresponding transverse sound velocities (Table 1).[31] Indeed,

Table 1. Physical Quantities of the 10-Bilayer PMMA-TiO_2 Superlattice Constituents and Substrate Used in the Theoretical Calculations[a]

parameter	TiO_2 layer[b]	PMMA layer	SiO_2 substrate
ρ (kg/m^3)	1900	1190	2480
c_L (m/s)	2900	2700	5660
c_T (m/s)	1800	1400	3250
d (nm)	57	40	1 mm
n	1.85	1.50	1.50

[a]Density (ρ), sound velocity (c_L), thickness (d), and refractive index (n). [b]Infiltrated.

the computed $c_{L,eff}$ = 2840m/s falls between the sound velocities of the constituent layers and is 6% smaller than the experimental c_L. Because of the finite size effect of the SL, a computation of the density of states (DOS) for the in-plane elastic excitations in the supported SL helped to identify the experimental acoustic mode.

Below the transverse sound velocity c_{T,SiO_2} = 3250 m/s of the substrate, there are two types of Rayleigh modes: one localized at the surface of the SL with sound velocity 1420 m/s (slightly below the mean $c_T \approx$ 1500 m/s of PMMA and TiO_2) and the second localized at the surface of the glass substrate with c_R = 3000 m/s (slightly below c_{T,SiO_2}). In addition, there are several discrete (or standing) modes confined in the SL. The calculation of DOS and displacement field for the present SL, shown respectively in panels b and c in Figure 3, was performed using the densities and sound velocities listed in Table 1.[32] Figure 3b gives the DOS vs the sound velocity at $q_\parallel$ = 0.0167 nm^{-1}, with (upper panel) and without (lower panel) the contribution of the glass substrate. The upper panel shows good agreement with the Brillouin spectra (Figure 3a), where the SiO_2 Rayleigh mode dominates the other SL guided modes. The lower panel shows a broad peak where the increase of DOS around the frequencies of the effective medium acoustic phonon ($c_{L,eff}$ = 2840 m/s, dashed arrow) is associated with the longitudinal guided mode (LGM).[33,34] Indeed, an analysis of the displacement field of this mode (Figure 3c) clearly shows that it is confined in the SL region and decreases exponentially in the substrate. Also, its longitudinal component (red line) is predominant in comparison with the transverse component (blue line). From a comparison between Figures 3a and 3b, and the fortuitous proximity of the values of c_R (= 3000 m/s) and $c_{L,eff}$ (= 2840 m/s), one can deduce the experimental c_L (= 3010 m/s) bears both contributions, rendering their discrimination ambiguous. Thus, the experimental c_L for in-plane propagation cannot be uniquely associated with the elastic properties of the two layers of the SL and is not free of substrate effects.

In the earlier investigation of the in-plane phonon propagation for a PMMA-TiO_2 SL, also on glass substrate, two dispersive phonons were resolved in the long wavelength limit ($q_\parallel d < 1$) using a photoacoustic technique.[22] Their dispersion in the multilayer structure was described assuming it was a single uniform layer with effective sound velocity 2870 m/s, being closer (15%) to the sound velocity in PMMA (2490 m/s in ref 21). In this low $q_\parallel$ range, the access to two dispersive elastic excitations allows the estimation of effective sound velocity, subject to the assumption of a uniform single layer. In the same context, the measured sound velocity 3020 m/s for a SiO_2−PMMA SL supported on glass substrate is very close to the effective value[14] and is affected to a lesser extent from the substrate because of the higher sound velocity of the SiO_2 nanoparticle phase c_{L,SiO_2} (= 3100 m/s) exceeding the c_R of the glass.

C. Hypersonic Phononic Band Gap (Normal to the SL).

Bragg interference band gap in SLs appears along the periodicity direction when the wavelength of the phonon propagating normal to the film is commensurate with the lattice constant, i.e., $q_\perp d \approx 1$.[10] The BLS spectra recorded for $q_\perp$ values close to the first BZ, at $\sim\pi/d$ = 0.032 nm^{-1}, deviate from the single peak structure of an effective medium acoustic propagation. Defect-free SLs display two-phonon branch structure at the Brillouin edge, whereas the presence of defects causes an increase of the number of resolved modes in the BLS spectrum.[21] In fact, Figure 4 (left panel) shows that three

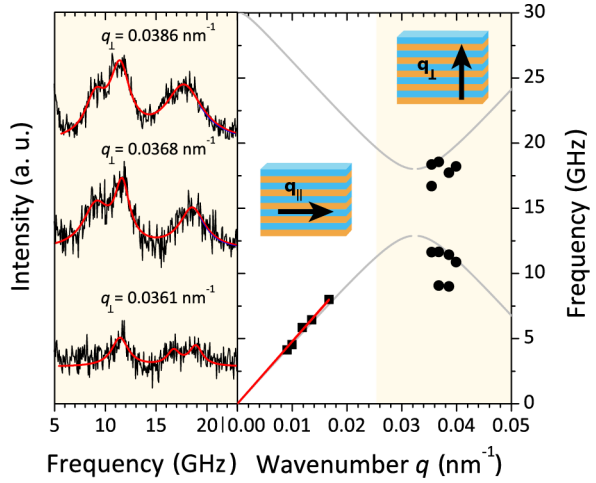

Figure 4. Left: BLS spectra recorded perpendicular to the substrate (parallel to the periodicity) at three wave vectors $q_\perp$ indicated in the left panel. Right: Dispersion relation for phonon propagation along the two orthogonal directions, parallel (squares) and perpendicular (circles) to the PMMA-TiO_2 SL layers. The dispersion for an infinite SL with $q_\perp$ is shown as a gray solid line, whereas the red solid line represents the linear (acoustic) dispersion for the in-plane propagation ($q_\parallel$) also shown in the right panel of Figure 3a.

Lorentzian shapes are necessary to represent the experimental BLS spectra and obtain the frequencies of the resolved modes at different wave vector modulus $q_\perp$. The dispersion along this direction reveals the anticipated Bragg-type phononic band gap centered at 15 GHz, with a bandwidth of ~5 GHz as shown in Figure 4 (right panel). The lower edge of the band gap is related to a standing wave with nodes located in the softer material (PMMA); the maximum amplitude of the displacement field is located in the TiO_2 layer. The opposite applies for the upper edge of the band gap, connected to the standing wave with nodes in TiO_2. Additional modes in the phononic band diagram are unequivocally related to the structural defects in the SL and their unique identification requires theoretical modeling of both the band diagram and BLS spectra.

The band structure is very sensitive to periodicity perturbations. The theoretical spectral shape considering the contribution of two cavity modes representing the defects is

DOI: 10.1021/acsami.5b01247
ACS Appl. Mater. Interfaces 2015, 7, 12488−12495

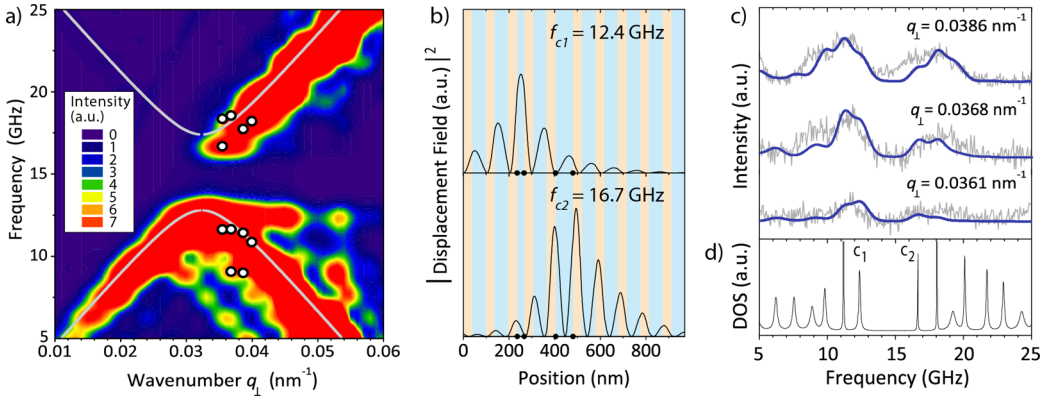

Figure 5. (a) Theoretical dispersion relation of an infinite SL (solid line) and Brillouin intensity, given as a color scale, for the PMMA-TiO_2 SL considering two cavity defects. (b) Square modulus of the displacement fields of the two cavity defects. The points in the position axis denote the limits of the defects.(c) Theoretical (solid line) and experimental BLS spectrum for three selected wave vectors $q_\perp$ (along the periodicity direction). (d) Total density of states (DOS), where c_1 and c_2 denote two cavity modes lying inside the band gap.

mapped in the contour plot of Figure 5, which accounts for the BLS intensity shown in a color scale (arbitrary units). The ideal case of an infinite defect-free lattice is represented by a solid gray line (Figure 5a). For the theoretical modeling, we considered two defects in the third and fifth layers of TiO_2 with thicknesses $d^3_{c_1}$ = 30 nm and $d^5_{c_2}$ = 75 nm, and the elastic parameters given in Table 1. The square modulus of the displacement field at the frequencies of modes labeled c_1 and c_2 is shown in Figure 5b. The maximum displacement occurs in the region of the considered defects, noted by dots in the position axis, and vanishes in the surface. Its frequencies are f_{c_1} (f_{c_2}) for the thin (thick) cavities with $f_{c_1} < f_{c_2}$. The two frequencies do respect the $f_c \approx 1/d_c$ dependence,[21] but as they fall on two different branches they appear to violate this relation. The total DOS integrated over the thickness (Figure 5d) identifies these cavity modes, and determines the Brillouin intensity as visualized in the BLS spectra of Figure 5c at $q_\perp$ = 0.0368 nm^{-1}. The theoretical BLS spectrum is represented by Lorentzian functions broadened by convolution with the instrumental function (~0.5 GHz).

In addition to the band gap structure, the effective medium behavior (low $q_\perp$ limit) along the periodicity direction is also predicted. The effective $c_{L\perp}$ can be obtained from the mean longitudinal modulus of the SL envisaged as a single uniform layer with $M_\perp = \rho c_{L\perp}^2$, where ρ (= 1610 kg/m^3) is the mean density. Because the SL modulus $M_\perp$ obeys Wood's law,[27] its value is obtained from the moduli of the constituent layers. Using the densities and the sound velocities of Table 1 and the volume fraction of the layers in SL, $M_\perp$ =11.8 GPa yielding $c_{L,\perp}$ = 2710 m/s. Interestingly, the effective medium sound velocities along the two symmetry directions are not the same; $c_{L,\perp}$ is about 5% lower than the in-plane $c_{L,eff}$ (= 2840 m/s). Assuming isotropic density, the effective in-plane elastic constant (C_{11}) is about 9% higher than the out-of-plane (C_{33}) component, asserting the anisotropic nature of the elastic tensor of the SL.[31] Access to direction dependent mechanical properties is not possible with conventional rheology or atomic force microscopy (AFM), but requires elastic wave propagation selectivity, feasible through the vector nature of the BLS technique.[29] As in the case of PMMA-SiO_2 SLs,[14,21] both phononic band diagram and the experimental BLS spectrum are well-represented with two adjustable parameters ($\rho^*_{TiO_2}$ and ratio of elasto-optic constants[35]) using all elastic moduli fixed to the values of the constituent TiO_2 and PMMA layers; the assumed number of defects and thicknesses are in conformity with the SEM images. These two successful cases allow for a reliable prediction of the elastic wave propagation in 1D phononic structures.

D. Photonic Band Structure. Further characterization of the SL was done via optical spectroscopy. When a monochromatic light is launched onto a periodic layered medium, with frequency in the range of the forbidden band gap, such a wave is evanescent and does not propagate through the medium. The energy is reflected, and the medium acts as a Bragg reflector. The peak reflectance for normal incidence occurs at the center of the forbidden band, given by $\lambda = 2n_{eff}d$.[36] In the present SL with an effective refractive index n_{eff} = 1.71 and lattice constant d = 97 nm, the peak should appear around 332 nm. Indeed, the photonic band gap was found experimentally in the range 315−360 nm (Figure 6a). As the films are supported by a glass substrate, a strong absorber in the UV region, experimental curves are affected by an error for $\lambda <$ 300 nm. At the laser wavelength (532 nm) used in the BLS experiment, the SL is transparent (arrow in Figure 6a) allowing for optimal transmittance required for strong BLS signal. The modulation of the SL optical behavior is noticeable in comparison to its constituents (dotted and dash-dotted lines), both being transparent in the visible.

To account for the band gap observed in the experimental transmittance, we have computed the photonic band structure of Figure 6b using the refractive indices n_{PMMA} = 1.5 and n_{TiO_2} = 1.85 for the constituent layers (Table 1).[37] We should note that n_{TiO_2} must be lower than the bulk anatase TiO_2 ($n_{TiO_2,bulk}$ = 2.5) due to the infilled PMMA. We have estimated n_{TiO_2} from n_{eff}, n_{PMMA} and the TiO_2 fraction in the SL, assuming a linear dependence. The computed photonic band structure exhibits a gap in the region of wavelengths 310−350 nm. The band gap opens because of the large mismatch in the dielectric constant ε ($\varepsilon \approx n^2$), or in other words, because of the difference in field energy location. At the edges of the band gap, the majority of the energy is localized either in the PMMA (lower part of band 2) or TiO_2 (upper part of band 1). The gap located in the UV region blocks those wavelengths and lets the rest, e.g., visible light, pass through the structure as seen in the photograph (inset of Figure 6b). Thus, a unidirectional phoxonic behavior (Figures 5a and 6) at different frequencies but with almost the

DOI: 10.1021/acsami.5b01247
ACS Appl. Mater. Interfaces 2015, 7, 12488−12495

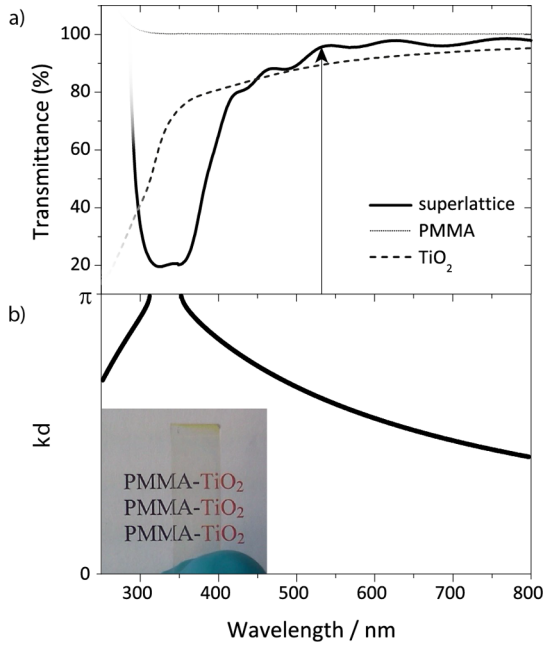

Figure 6. (a) UV/vis spectrum of the ten bilayer PMMA/TiO_2 SL (solid). The PMMA (dotted) and TiO_2 nanoparticle (dash-dot line) films are also shown with a distinct transmittance than the SL. The wavelength of the probing light (532 nm) is pointed by an arrow. (b) Calculated band structure of the infinite SL. Inset: picture of the sample showing its transparency in the visible region.

same wavelengths for the elastic and electromagnetic waves is realized and justified for a hybrid SL.

CONCLUSIONS

We have studied by Brillouin light scattering (BLS) the elastic wave propagation in supported one-dimensional PMMA-TiO_2 multilayer structure (superlattice, SL) along and normal to the periodicity direction. The isotropic wave propagation in the constituent layers becomes direction dependent in the SL, with rich dispersion frequency vs. wave vector relations. Normal to the periodicity (in-plane) phonon propagation depends on the elastic mechanical properties of the constituent layers but also on the glass substrate in the case of finite SL thickness. The observed acoustic mode is not necessarily identified with the longitudinal acoustic phonon of the effective SL medium, fully determined by the composition and properties of the constituent layers. Instead, it relates to the predominantly longitudinal guided mode (LGM) localized in the SL as reflected by the computed displacement fields of the propagating modes along the layers. Based on the density-of-states (DOS) calculations, the LGM frequency of this SL is higher than the frequency of the effective medium phonon. The proximity of the two modes depends on the longitudinal sound velocities in the constituent layers relative to the transverse velocity of the glass and the thickness of the SL. Hence, the extraction of the material elastic properties from the experimental acoustic mode is not straightforward.

For the elastic and electromagnetic wave propagation along the periodicity direction studied by BLS and optical reflectance, a dual large band gap in the hypersonic (GHz) and near UV frequencies is realized for the first time in hybrid SLs. Although the spin-coating technique provides a facile fabrication of SLs with large range of materials, however the structure coherence is low compared to semiconductor SLs using MBE fabrication. The width of the band gaps is rather robust to such thickness variation but distinct defects are manifested in the BZ edge as localized modes. The theoretical representation of the dispersion band diagram, as well as of the BLS spectra, allows the identification of cavity defects and the elastic properties of the constituent layers. Surprisingly, the sound velocity in the TiO_2 layer is marginally higher than in PMMA layer and hence the observed large band gap essentially reflects the density contrast. For the effective medium elastic modulus along the symmetry direction, a low (~9%) mechanical anisotropy is revealed.

This is the first realization of a unidirectional phoxonic hybrid SL occurring at similar phonon ($\Lambda = 2\pi/0.032$ nm) and photon ($\lambda = 332/n_{eff}$ nm) wavelengths ~200 nm, and complements the recent report on porous silicon SL.[15] However, in the present BLS experiment with a laser wavelength at 532 nm the phonon-photon coupling must be weak. To the best of our knowledge, there are only theoretical works on active 1D phoxonic structures.[38−40] The present experimental and theoretical study provides a thorough understanding of 1D phoxonic structures necessary to access fundamental concepts such as opto-acoustic interactions, phonon and photon confinement for sound amplification and Bragg mirrors. Alternative fabrications techniques such as direct ink writing[41] can be examined to further improve and extend the range of hybrid SLs, which is a step forward from the conventional semiconductor-based structures.

MATERIALS AND METHODS

Nanoparticles. 3,4-Dihydroxyhydrocinnamic acid (DHCA) functionalized TiO_2 nanoparticles were synthesized by hydrolyzing 20.6 mL of titanium isopropoxide in 37 mL of Milli-Q water and stirring for 1 h. The resulting white precipitate was filtered and dried in air before transferring into a stainless steel autoclave containing 0.96 g of DHCA and 12.8 mL of 5 wt % tetramethylammonium hydroxide solution (TMAOH). The autoclave was sealed and heated for 6 h at 120 °C and 4.5 h at 195 °C. The particles are composed of the anatase phase with mass density of 3.9 g/mL.

Superlattice. It was added 6.78 mL of 14% NH_3 and 100 μL of 10 wt % sodium dodecyl sulfate were added to 3.22 mL of the as-prepared nanoparticle solution. Ten alternating layers of 2.2 wt % of PMMA (poly[methyl-methacrylate], Acros Organics) solution in toluene and TiO_2 solution was spin coated on a glass substrate (spin coating parameters: v = 5000 rpm, t = 20 s.; ACL = 5000 rpm/s), with a heat treatment of 100 °C for 15 min after each layer.

For the TiO_2-infiltrated film, we used the TiO_2 solution and a 1 wt % PMMA solution in toluene. The spin-coating procedure was the same as for the SL, with a total number of 13 layers of TiO_2, which amounts to a thickness of ~1 μm.

Brillouin Light Scattering and Optical Spectroscopy. BLS is a noninvasive technique which utilizes the scattering of an incident probing laser beam from thermally activated density fluctuations (phonons) in transparent materials along a certain direction. The probing wave vector direction is selected with the scattering geometry, and its wavenumber $q_{\parallel} = 4\pi/\lambda \sin(\theta/2)$ is dependent on the wavelength of the probing beam λ = 532 nm and the scattering angle θ for propagation parallel to the substrate plane. The probing wave vector $q_{\perp}(n)$ perpendicular to the substrate is depending on the refractive index, n, and the analytical expression can be found elsewhere.[14] The BLS spectrum for homogeneous materials consists of a double frequency shift ($\pm f$) at GHz frequencies, resolved by a tandem Fabry-Perót interferometer (JRS Instruments), whereas for structured materials, a more complex spectrum arises. The dispersion relation $f(q)$ reveals much information such as sound velocity, effective refractive index, and avoided frequency regions (band gaps) in the GHz regime.

DOI: 10.1021/acsami.5b01247
ACS Appl. Mater. Interfaces 2015, 7, 12488−12495

The optical transmittance of the SLs was checked by an UV/vis spectrometer (Varian, Cary 5G UV/vis−NIR spectrometer) at normal incidence.

Electron Microscopy. The morphology and microstructure of the SL were characterized by a scanning electron microscope (SEM, LEO Gemini 1530) at 0.7 kV (Figure 1). The measured thickness of the PMMA (TiO_2) layers is 40 ± 5 (57 ± 7) nm. A deviation of this value is observable, especially in certain layers that are subsequently treated as defects, which are of special importance in the theoretical description of the band structure.

Nanoparticles were drop-coated on a carbon-coated copper grid from an ethanolic solution and measured with at acceleration voltage of 120 kV with a transmission electron microscope (TEM, JEOL 1400). Nanoparticles are spherical, with an average diameter of (7 ± 2) nm.

Theoretical Modeling. The computation of BLS spectra is based on the calculation of DOS utilizing Green's function technique. The reader is referred to Suplemental Information of ref 21.

AUTHOR INFORMATION

Corresponding Author

*E-mail: fytas@mpip-mainz.mpg.de.

Author Contributions

†E.A. and H.H. contributed equally. The manuscript was written through contributions of all authors. All authors have given approval to the final version of the manuscript.

Notes

The authors declare no competing financial interest.

ACKNOWLEDGMENTS

HH thanks the International Research Training Group (IRTG) 1404 Self Organized Materials for Optoelectronics supported by the Deutsche Forschungsgemeinschaft. HH and EAR thank the Max Planck Society for financial support. The work was supported partially by Aristeia Program-285 (EU, GSST Greece).

DEDICATION

The authors dedicate this manuscript to Prof. Dr. Manfred Stamm on the occasion of his 65th birthday.

ABBREVIATIONS

SL, superlattice
PMMA, poly(methyl-methacrylate)
BLS, Brillouin light scattering
BZ, Brillouin zone
LGM, longitudinal guided modes
DOS, density of states

REFERENCES

(1) Yoon, J.; Lee, W.; Caruge, H. M.; Bawendi, M.; Thomas, E. L.; Kooi, S.; Prasad, P. N. Defect-Mode Mirrorless Lasing in Dye-Doped Organic/Inorganic Hybrid One-Dimensional Photonic Crystal. *Appl. Phys. Lett.* **2006**, *88*, 091102.

(2) Kang, Y.; Walish, J. J.; Gorishnyy, T.; Thomas, E. L. Broad-Wavelength-Range Chemically Tunable Block-Copolymer Photonic Gels. *Nat. Mater.* **2007**, *6*, 957−960.

(3) Lucklum, R.; Ke, M.; Zubtsov, M. Two-Dimensional Phononic Crystal Sensor Based on a Cavity Mode. *Sens. Actuators, B* **2012**, *171*−*172*, 271−277.

(4) Savić, I.; Donadio, D.; Gygi, F.; Galli, G. Dimensionality and Heat Transport in Si-Ge Superlattices. *Appl. Phys. Lett.* **2013**, *102*, 073113.

(5) Chang, C. W.; Okawa, D.; Majumdar, A.; Zettl, A. Solid-State Thermal Rectifier. *Science* **2006**, *314*, 1121−1124.

(6) Maldovan, M. Sound and Heat Revolutions in Phononics. *Nature* **2013**, *503*, 209−217.

(7) Urbas, A.; Sharp, R.; Fink, Y.; Thomas, E. L.; Xenidou, M.; Fetters, L. J. Tunable Block Copolymer/Homopolymer Photonic Crystals. *Adv. Mater.* **2000**, *12*, 812−814.

(8) Piunova, V. A.; Miyake, G. M.; Daeffler, C. S.; Weitekamp, R. A.; Grubbs, R. H. Highly Ordered Dielectric Mirrors via the Self-Assembly of Dendronized Block Copolymers. *J. Am. Chem. Soc.* **2013**, *135*, 15609−15616.

(9) Lee, J. H.; Koh, C. Y.; Singer, J. P.; Jeon, S. J.; Maldovan, M.; Stein, O.; Thomas, E. L. 25th Anniversary Article: Ordered Polymer Structures for the Engineering of Photons and Phonons. *Adv. Mater.* **2014**, *26*, 532−569.

(10) Gomopoulos, N.; Maschke, D.; Koh, C. Y.; Thomas, E. L.; Tremel, W.; Butt, H.-J.; Fytas, G. One-Dimensional Hypersonic Phononic Crystals. *Nano Lett.* **2010**, *10*, 980−984.

(11) Walker, P. M.; Sharp, J. S.; Akimov, A. V.; Kent, A. J. Coherent Elastic Waves in a One-Dimensional Polymer Hypersonic Crystal. *Appl. Phys. Lett.* **2010**, *97*, 073106.

(12) Ogata, T.; Yagi, R.; Nakamura, N.; Kuwahara, Y.; Kurihara, S. Modulation of Polymer Refractive Indices with Diamond Nanoparticles for Metal-Free Multilayer Film Mirrors. *ACS Appl. Mater. Interfaces* **2012**, *4*, 3769−3772.

(13) Narayanan, S.; Choi, J.; Porter, L.; Bockstaller, M. R. Flexible Transparent Metal/Polymer Composite Materials Based on Optical Resonant Laminate Structures. *ACS Appl. Mater. Interfaces* **2013**, *5*, 4093−4099.

(14) Schneider, D.; Liaqat, F.; El Boudouti, E. H.; El Hassouani, Y.; Djafari-Rouhani, B.; Tremel, W.; Butt, H.-J.; Fytas, G. Engineering the Hypersonic Phononic Band Gap of Hybrid Bragg Stacks. *Nano Lett.* **2012**, *12*, 3101−3108.

(15) Parsons, L. C.; Andrews, G. T. Off-Axis Phonon and Photon Propagation in Porous Silicon Superlattices Studied by Brillouin Spectroscopy and Optical Reflectance. *J. Appl. Phys.* **2014**, *116*, 033510.

(16) Trigo, M.; Bruchhausen, A.; Fainstein, A.; Jusserand, B.; Thierry-Mieg, V. Confinement of Acoustical Vibrations in a Semiconductor Planar Phonon Cavity. *Phys. Rev. Lett.* **2002**, *89*, 227402.

(17) Trodahl, H. J.; Santos, P. V.; Williams, G. V. M; Bittar, A. Raman Scattering from Surface and Bulk Acoustic Phonons in Capped Superlattices. *Phys. Rev. B* **1989**, *40*, 8577−8580.

(18) Pu, N. W.; Bokor, J. Study of Surface and Bulk Acoustic Phonon Excitations in Superlattices Using Picosecond Ultrasonics. *Phys. Rev. Lett.* **2003**, *91*, 076101.

(19) Trigo, M.; Eckhause, T. A.; Reason, M.; Goldman, R. S.; Merlin, R. Observation of Surface-Avoiding Waves: A New Class of Extended States in Periodic Media. *Phys. Rev. Lett.* **2006**, *97*, 124301.

(20) Hou, C. G.; Zhang, V. L.; Lim, H. S.; Ng, S. C.; Kuok, M. H.; Deng, J.; Wang, S. J. Band Structures of Surface Acoustic Waves in Nanostructured Phononic Crystals with Defects. *Appl. Phys. Lett.* **2014**, *105*, 243104.

(21) Schneider, D.; Liaqat, F.; El Boudouti, E. H.; El Abouti, O.; Tremel, W.; Butt, H.-J.; Djafari-Rouhani, B.; Fytas, G. Defect-Controlled Hypersound Propagation in Hybrid Superlattices. *Phys. Rev. Lett.* **2013**, *111*, 164301.

(22) Saini, G.; Pezeril, T.; Torchinsky, D. H.; Yoon, J.; Kooi, S. E.; Thomas, E. L.; Nelson, K. A. Pulsed Laser Characterization of Multicomponent Polymer Acoustic and Mechanical Properties in the Sub-GHz Regime. *J. Mater. Res.* **2006**, *22*, 719−723.

(23) Manzanares-Martínez, B.; Sánchez-Dehesa, J.; Hakansson, A.; Cervera, F.; Ramos-Mendieta, F. Experimental Evidence of Omnidirectional Elastic Bandgap in Finite One-Dimensional Phononic Systems. *Appl. Phys. Lett.* **2004**, *85*, 154−156.

(24) Cheng, W.; Sainidou, R.; Burgardt, P.; Stefanou, N.; Kiyanova, A.; Efremov, M.; Fytas, G.; Nealey, P. F. Elastic Properties and Glass Transition of Supported Polymer Thin Films. *Macromolecules* **2007**, *40*, 7283−7290.

DOI: 10.1021/acsami.5b01247
ACS Appl. Mater. Interfaces 2015, 7, 12488−12495

(25) Gomopoulos, N.; Cheng, W.; Efremov, M.; Nealey, P. F.; Fytas, G. Out-of-Plane Longitudinal Elastic Modulus of Supported Polymer Thin Films. *Macromolecules* **2009**, *42*, 7164−7167.
(26) Bandhu, R. S.; Zhang, X.; Sooryakumar, R.; Bussmann, K. Acoustic Vibrations in Free-Standing Double Layer Membranes. *Phys. Rev. B* **2004**, *70*, 075409.
(27) Wood, A. B. *A Textbook of Sound*; Neill & Co.: Edinburgh, U.K., 1930.
(28) Torrent, D.; Sánchez-Dehesa, J. Acoustic Metamaterials for New Two-Dimensional Sonic Devices. *New J. Phys.* **2007**, *9*, 323.
(29) Gomopoulos, N.; Saini, G.; Efremov, M.; Nealey, P. F.; Nelson, K.; Fytas, G. Non- Destructive Probing of Mechanical Anisotropy in Polyimide Films at Nanoscale. *Macromolecules* **2010**, *43*, 1551−1555.
(30) Cuffe, J.; Chávez, E.; Shchepetov, A.; Chapuis, P. O.; El Boudouti, E. H.; Alzina, F.; Kehoe, T.; Gomis-Bresco, J.; Dudek, D.; Pennec, Y.; Djafari-Rouhani, B.; Prunnila, M.; Ahopelto, J.; Sotomayor Torres, C. Phonons in Slow Motion: Dispersion Relations in Ultra-Thin Si Membranes. *Nano Lett.* **2012**, *12*, 3569−3573.
(31) Djafari-Rouhani, B.; Sapriel, J. Effective Dielectric and Photoelastic Tensors of Superlattices in the Long-Wavelength Regime. *Phys. Rev. B* **1986**, *34*, 7114−7117.
(32) El Boudouti, E. H.; Djafari-Rouhani, B.; Akjouj, A.; Dobrzynski, L. Acoustic Waves in Solid and Fluid Layered Materials. *Surf. Sci. Rep.* **2009**, *64*, 471−594.
(33) Chirita, M.; Sooryakumar, R.; Venugopal, R.; Wan, J.; Melloch, M. R. Acoustic Barriers and Observation of Guided Elastic Waves in GaN-AlN Structures by Brillouin Scattering. *Phys. Rev. B* **2001**, *63*, 205302.
(34) Hillebrands, B.; Lee, S.; Stegeman, G. I.; Cheng, H.; Potts, J. E.; Nizzoli, F. Evidence for the Existence of Guided Longitudinal Acoustic Phonons in ZnSe Films on GaAs. *Phys. Rev. Lett.* **1988**, *60*, 832−835.
(35) The ratio of elasto-optic constants for PMMA and TiO_2 was assumed as $p_{PMMA}/p_{TiO_2} = 1.9$.
(36) Yeh, P. *Optical Waves in Layered Media*, 2nd ed.; Wiley: New York, 2005.
(37) Joannopoulos, J. D.; Johnson, S. G.; Winn, J. N.; Meade, R. D. *Photonic Crystals: Molding the Flow of Light*, 2nd ed; Princeton University Press: Princeton, NJ, 2008.
(38) Maldovan, M.; Thomas, E. L. Simultaneous Localization of Photons and Phonons in Two-Dimensional Periodic Structures. *Appl. Phys. Lett.* **2006**, *88*, 251907.
(39) Martínez, A. Phoxonic Crystals: Tailoring the Light-Sound Interaction at the Nanoscale. *Proc. SPIE* **2013**, *8632*, No. 8632OW.
(40) Papanikolaou, N.; Psarobas, I. E.; Stefanou, N.; Djafari-Rohuhani, B.; Bonello, B.; Laude, V. Light Modulation in Phoxonic Nanocavities. *Microelectron. Eng.* **2012**, *90*, 155−158.
(41) George, M. C.; Mohraz, A.; Piech, M.; Bell, N. S.; Lewis, J. A.; Braun, P. V. Direct Laser Writing of Photoresponsive Colloids for Microscale Patterning of 3D Porous Structures. *Adv. Mater.* **2009**, *21*, 66−70.

DOI: 10.1021/acsami.5b01247
ACS Appl. Mater. Interfaces 2015, 7, 12488−12495